

Statefinder diagnostic for holographic dark energy model

Xin Zhang

*Institute of High Energy Physics, Chinese Academy of Sciences
P.O.Box 918(4), Beijing 100049, People's Republic of China*

zhangxin@mail.ihep.ac.cn

Abstract

In this paper we study the holographic dark energy model proposed by Li from the statefinder viewpoint. We plot the evolutionary trajectories of the model with $c = 1$ in the statefinder parameter-planes. The statefinder diagrams characterize the properties of the holographic dark energy and show the discrimination between this scenario and other dark energy models. We also perform a statefinder diagnostic to the holographic dark energy model in cases of different c which given by three fits to observational data. The result indicates that from the statefinder viewpoint c plays a significant role in this model and should thus be determined seriously by future high precision experiments.

Physicists and astronomers begin to consider the dark energy cosmology seriously and to explore the nature of dark energy actively since the expansion of our universe is proven to be accelerating at present time by the Type Ia supernovae observations [1]. The analysis of cosmological observations, in particular of the WMAP (Wilkinson Microwave Anisotropy Probe) experiment [2], indicates that dark energy occupies about 2/3 of the total energy of our universe, and dark matter about 1/3. The accelerated expansion of the present universe is attributed to that dark energy is an exotic component with negative pressure, and many models have been constructed for interpreting or describing this component. It should be pointed out that the hottest candidates for dark energy are the cosmological constant (or vacuum energy) [3] and the quintessence scalar field [4]. However, as is well known, there are two difficulties arise from all of these scenarios, namely the two dark energy (or cosmological constant) problems – the fine-tuning problem and the cosmic coincidence problem. The fine-tuning problem asks why the dark energy density today is so small compared to typical particle scales. The dark energy density is of order 10^{-47}GeV^4 , which appears to require the introduction of a new mass scale 14 or so orders of magnitude smaller than the electroweak scale. The second difficulty, the cosmic coincidence problem, states: Since the energy densities of dark energy and dark matter scale so differently during the expansion of the universe, why are they nearly equal today? To get this coincidence, it appears that their ratio must be set to a specific, infinitesimal value in the very early universe.

Recently, considerable interest has been stimulated in explaining the observed dark energy by the holographic dark energy model. For an effective field theory in a box of size L , with UV cut-off Λ_c the entropy S scales extensively, $S \sim L^3 \Lambda_c^3$. However, the peculiar thermodynamics of black hole [5] has led Bekenstein to postulate that the maximum entropy in a box of volume L^3 behaves nonextensively, growing only as the area of the box, i.e. there is a so-called Bekenstein entropy bound, $S \leq S_{BH} \equiv \pi M_p^2 L^2$. This nonextensive scaling suggests that quantum field theory breaks down in large volume. To reconcile this breakdown with the success of local quantum field theory in describing observed particle phenomenology, Cohen et al. [6] proposed a more restrictive bound – the energy bound. They pointed out that in quantum field theory a short distance (UV) cut-off is related to a long distance (IR) cut-off due to the limit set by forming a black hole. In the other words, if the quantum zero-point energy density ρ_Λ is relevant to a UV cut-off, the total energy of the whole system with size L should not exceed the mass of a black hole of the same size, thus we have $L^3 \rho_\Lambda \leq LM_p^2$, this means that the maximum entropy is in order of $S_{BH}^{3/4}$. When we take the whole universe into account, the vacuum energy related to this holographic principle [7] is viewed as dark energy, usually dubbed holographic dark energy. The largest IR cut-off L

is chosen by saturating the inequality so that we get the holographic dark energy density

$$\rho_\Lambda = 3c^2 M_p^2 L^{-2} , \quad (1)$$

where c is a numerical constant, and $M_p \equiv 1/\sqrt{8\pi G}$ is the reduced Planck mass. If we take L as the size of the current universe, for instance the Hubble scale H^{-1} , then the dark energy density will be close to the observed data. However, Hsu [8] pointed out that this yields a wrong equation of state for dark energy. Li [9] subsequently proposed that the IR cut-off L should be taken as the size of the future event horizon

$$R_h(a) = a \int_t^\infty \frac{dt'}{a(t')} = a \int_a^\infty \frac{da'}{H(a')a'^2} , \quad (2)$$

then the problem can be solved nicely and the holographic dark energy model can thus be constructed successfully. The holographic dark energy scenario may provide natural solutions to both dark energy problems at the same time as indicated in Ref. [9]. Some speculations on the deep reasons of the holographic dark energy were considered by several authors [10]. Further studies on this model can also be found in Refs. [11–17].

However, on the other hand, since more and more dark energy models have been constructed for interpreting or describing the cosmic acceleration, the problem of discriminating between the various contenders is now emergent. In order to be able to differentiate between those competing cosmological scenarios involving dark energy, a sensitive and robust diagnostic for dark energy models is a must. For this purpose a diagnostic proposal that makes use of parameter pair $\{r, s\}$, the so-called “statefinder”, was introduced by Sahni et al. [18]. The statefinder probes the expansion dynamics of the universe through higher derivatives of the expansion factor \ddot{a} and is a natural companion to the deceleration parameter q which depends upon \ddot{a} . The statefinder pair $\{r, s\}$ is defined as follows

$$r \equiv \frac{\ddot{a}}{aH^3}, \quad s \equiv \frac{r-1}{3(q-1/2)} . \quad (3)$$

The statefinder is a “geometrical” diagnostic in the sense that it depends upon the expansion factor and hence upon the metric describing space-time.

Trajectories in the $s - r$ plane corresponding to different cosmological models exhibit qualitatively different behaviors. The spatially flat LCDM (cosmological constant Λ with cold dark matter) scenario corresponds to a fixed point in the diagram

$$\{s, r\} \Big|_{\text{LCDM}} = \{0, 1\} . \quad (4)$$

Departure of a given dark energy model from this fixed point provides a good way of establishing the “distance” of this model from LCDM [18,19]. As demonstrated in Refs. [18–22]

the statefinder can successfully differentiate between a wide variety of dark energy models including the cosmological constant, quintessence, the Chaplygin gas, braneworld models and interacting dark energy models. We can clearly identify the “distance” from a given dark energy model to the LCDM scenario by using the $r(s)$ evolution diagram.

The current location of the parameters s and r in these diagrams can be calculated in models, and on the other hand it can also be extracted from data coming from SNAP (SuperNovae Acceleration Probe) type experiments. Therefore, the statefinder diagnostic combined with future SNAP observations may possibly be used to discriminate between different dark energy models.

In this paper we apply the statefinder diagnostic to the holographic dark energy model. The statefinder can also be used to diagnose different cases of the model. Analysis of the observational data provides constraints on the holographic dark energy model. A direct comparison of the present available Type Ia supernovae data with the holographic dark energy model was undertaken recently [12]. Constraints on the parameters of the model arising from the observations of cosmic microwave background (CMB) was studied [14]. The possible connection between the holographic dark energy and the low- l CMB multipoles was analyzed [15,16]. However, it is remarkable that the values of the free parameter c determined by different authors are so different. We use the statefinder to diagnose these different cases, and the result shows that the parameter c plays an important role in the model and thus should be considered seriously and should be determined accurately by future high precision experiments.

In what follows we will calculate the statefinder parameters for the holographic dark energy model and plot the evolutionary trajectories of the model in the statefinder parameter-planes. We now consider a spatially flat FRW (Friedmann-Robertson-Walker) universe with matter component ρ_m (including both baryon matter and cold dark matter) and holographic dark energy component ρ_Λ , the Friedmann equation reads

$$1 = \Omega_m + \Omega_\Lambda , \quad (5)$$

where $\Omega_m = \Omega_m^0 H_0^2 H^{-2} a^{-3}$ and $\Omega_\Lambda = c^2 H^{-2} R_h^{-2}$ are relative energy densities of matter and dark energy, respectively, expressed as fractions of the critical density $\rho_c = 3M_p^2 H^2$. By using $R_h = c/H\sqrt{\Omega_\Lambda}$ and the definition of the event horizon (2), we get

$$\int_x^\infty \frac{dx'}{H(a')a'} = \frac{c}{H(a)a\sqrt{\Omega_\Lambda}} , \quad (6)$$

where $x = \ln a$. We notice that the Friedmann equation implies

$$\frac{1}{H(a)a} = \sqrt{a(1 - \Omega_\Lambda)} \frac{1}{H_0\sqrt{\Omega_m^0}} . \quad (7)$$

Combining (6) and (7), one obtains the relation

$$\int_x^\infty e^{x'/2} \sqrt{1 - \Omega_\Lambda} dx' = ce^{x/2} \sqrt{\frac{1}{\Omega_\Lambda} - 1} . \quad (8)$$

Then taking derivative with respect to x in both sides of the above relation, we get

$$\Omega'_\Lambda = \Omega_\Lambda(1 - \Omega_\Lambda)\left(1 + \frac{2}{c}\sqrt{\Omega_\Lambda}\right) , \quad (9)$$

where the prime denotes the derivative with respect to x . This differential equation describes the behavior of the holographic dark energy completely, and it can be solved analytically [9,12].

From the energy conservation equation of the dark energy, the equation of state of the dark energy can be expressed as

$$w = -1 - \frac{1}{3} \frac{d \ln \rho_\Lambda}{d \ln a} . \quad (10)$$

Then making use of the formula $\rho_\Lambda = \frac{\Omega_\Lambda}{1 - \Omega_\Lambda} \rho_m^0 a^{-3}$ and the differential equation of Ω_Λ (9), the equation of state for the holographic dark energy can be given

$$w = -\frac{1}{3} \left(1 + \frac{2}{c} \sqrt{\Omega_\Lambda}\right) . \quad (11)$$

Also, we can give the change rate of w with respect to $x = \ln a$,

$$w' = -\frac{1}{3c} \sqrt{\Omega_\Lambda} (1 - \Omega_\Lambda) \left(1 + \frac{2}{c} \sqrt{\Omega_\Lambda}\right) . \quad (12)$$

It can be seen clearly that the equation of state of the holographic dark energy satisfies $-(1 + 2/c)/3 \leq w \leq -1/3$ due to $0 \leq \Omega_\Lambda \leq 1$. If we take $c = 1$, the behavior of the holographic dark energy will be more and more like a cosmological constant with the expansion of the universe, and the ultimate fate of the universe will be entering the de Sitter phase in the far future. As is shown in Ref. [9], if one puts the parameter $\Omega_\Lambda^0 = 0.73$ into (11), then a definite prediction of this model, $w^0 = -0.903$, will be given.

The statefinder parameters r and s can also be expressed as

$$r = 1 + \frac{9}{2} w(1 + w) \Omega_\Lambda - \frac{3}{2} w' \Omega_\Lambda , \quad (13)$$

$$s = 1 + w - \frac{1}{3} \frac{w'}{w} . \quad (14)$$

Thus, using (11) and (12) we can give these parameters in terms of Ω_Λ ,

$$r = 1 - \Omega_\Lambda - \frac{1}{2c} \Omega_\Lambda^{3/2} (1 + \Omega_\Lambda) + \frac{1}{c^2} \Omega_\Lambda^2 (3 - \Omega_\Lambda) , \quad (15)$$

$$s = \frac{2}{3} - \frac{1}{3c} \sqrt{\Omega_\Lambda(3 - \Omega_\Lambda)} . \quad (16)$$

Another important parameter in the statefinder diagnostic is the deceleration parameter $q = -\ddot{a}/aH^2$, we also express it in terms of Ω_Λ ,

$$q = \frac{1}{2} - \frac{1}{2}\Omega_\Lambda - \frac{1}{c}\Omega_\Lambda^{3/2} . \quad (17)$$

Though the relations between these statefinder parameters, namely the functions $r(s)$ and $r(q)$, can be derived analytically in principle, we do not give the expressions here due to the complexity of the formulae. Making the parameter Ω_Λ vary from 0 to 1, one can easily get the evolutionary trajectories in the statefinder parameter-planes of this model. As an example, we plot the statefinder diagrams in the $s - r$ plane and $q - r$ plane corresponding to the case $c = 1$ in Fig.1 and Fig.2.

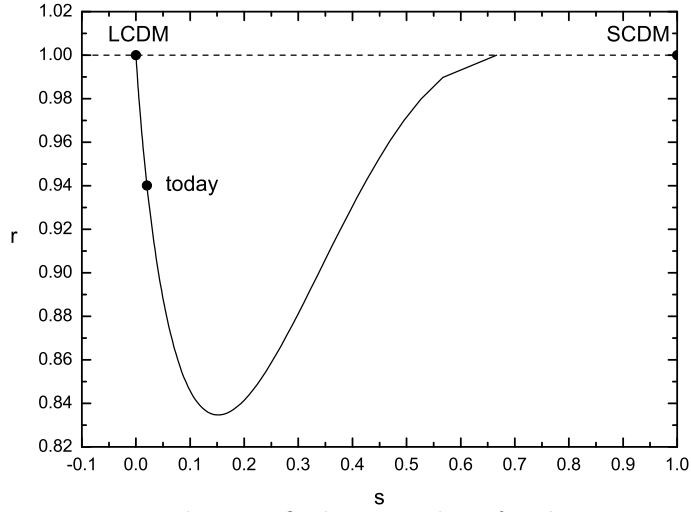


FIG. 1. Evolution trajectory in the statefinder $s-r$ plane for the case $c = 1$. LCDM corresponds to a fixed point $(0, 1)$, and SCDM corresponds to $(1, 1)$. For the holographic dark energy model, s monotonically decreases from $2/3$ to 0, whereas r first decreases from 1 to a minimum value, then rises to 1. The coordinate of today's point is $(0.02, 0.94)$, thus the 'distance' from this model to the LCDM can be easily identified in this diagram.

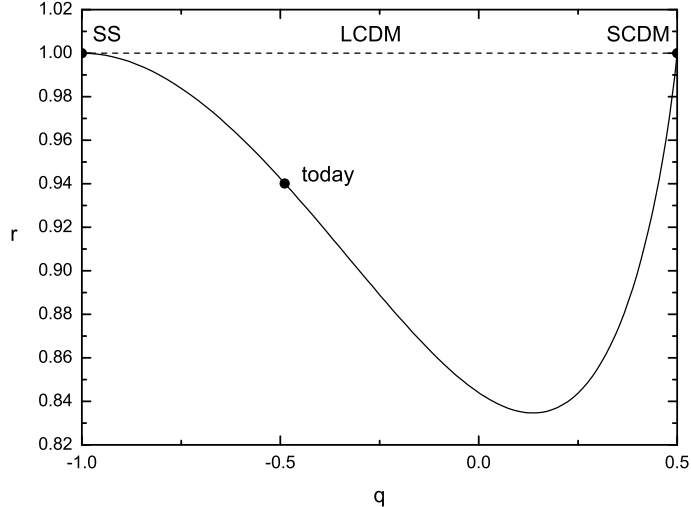


FIG. 2. Evolution trajectory in the statefinder $q - r$ plane for the case $c = 1$. The solid line represents the holographic dark energy model, and the dashed line the LCDM as comparison. Both models diverge at the same point in the past $(0.5, 1)$ which corresponds to a matter dominated universe (SCDM), and converge to the same point in the future $(-1, 1)$ which corresponds to the steady state model (SS) - the de Sitter expansion. The point of today in this plane locates at $(-0.49, 0.94)$.

The statefinder diagnostic can discriminate between various dark energy models effectively. Different cosmological models involving dark energy exhibit qualitatively different evolution trajectories in the $s - r$ plane. For example, the LCDM scenario corresponds to the fixed point $s = 0, r = 1$ as shown in (4), and the SCDM (standard cold dark matter) scenario corresponds to the point $s = 1, r = 1$. For the so-called “quiescence” models (w is a constant), the trajectories are some vertical segments, i.e. r decreases monotonically from 1 to $1 + \frac{2}{3}w(1 + w)$ while s remains constant at $1 + w$ [18]. The quintessence (inverse power law) tracker models and the Chaplygin gas models have typical trajectories similar to arcs of a parabola (upward and downward) lying in the regions $s > 0, r < 1$ and $s < 0, r > 1$, respectively [18–20]. The coupled quintessence models exhibit more complicated trajectories as shown in Ref. [22]. For the holographic dark energy scenario, as shown in Fig.1 ($c = 1$ case), commences its evolution from $s = 2/3, r = 1$, through an arc segment, and ends it at the LCDM fixed point ($s = 0, r = 1$) in the future. We see clearly from this diagram that s decreases monotonically to zero, while r first decreases to a minimum value then increases to unity. According to the holographic dark energy model, the current universe corresponds to a point $s = 0.02, r = 0.94$ in the plane. Therefore, the “distance” from this model to the LCDM scenario can be identified explicitly. The distinctive trajectories which various dark energy scenarios follow in the $s - r$ plane demonstrate quite strikingly the contrasting behavior of dark energy models.

As a complementarity, Fig.2 shows another statefinder diagram — the $r(q)$ evolutionary

trajectory. From this figure, we clearly see that both LCDM scenario and holographic dark energy model commence evolving from the same point in the past ($q = 0.5, r = 1$) which corresponds to a matter dominated SCDM universe, and end their evolution at the same common point in the future ($q = -1, r = 1$) which corresponds to a steady state cosmology (SS) — the de Sitter expansion. The trajectories of LCDM model and holographic dark energy model follow are horizontal segment and arc segment, respectively, in this diagram. In the holographic dark energy model, the point of today in this plane locates at $q = -0.49, r = 0.94$.

Theoretically, it has been argued in Ref. [9] that, for the numerical parameter, $c = 1$ is a good choice. However, one prefers to consider c as a free parameter of the model when performing a fit to observational data. Actually, if $c < 1$, the holographic dark energy will behave like a Quintom proposed recently in Ref. [23], the amazing feature of which is that the equation of state of dark energy component w crosses -1 , i.e. it is larger than -1 in the past while less than -1 near today. The recent fits to current SN Ia data with parametrization of the equation of state of dark energy find the Quintom type dark energy is mildly favored [24]. Usually the Quintom dark energy model is realized in terms of double fields – a quintessence and a phantom, which dominate at earlier time and today respectively [25,26]. However, the holographic dark energy in the case $c < 1$ provides a more natural realization of the Quintom picture. While, if $c > 1$, the equation of state of dark energy will be always larger than -1 such that the universe avoids entering the de Sitter phase and the Big Rip phase. Hence, we see explicitly, the determining of the value of c is a key point to the feature of the holographic dark energy and the ultimate fate of the universe as well. However, in the recent fit studies, different groups gave different values to c . A direct fit of the present available SNe Ia data with this holographic model indicates that the best fit result is $c = 0.21$ [12]. Recently, by calculating the average equation of state of the dark energy and the angular scale of the acoustic oscillation from the BOOMERANG and WMAP data on the CMB to constrain the holographic dark energy model, the authors show that the reasonable result is $c \sim 0.7$ [14]. In addition, the holographic dark energy model has also been used to investigate the suppression of the power at low multipoles in the CMB spectrum [15]. In the study of the constraints on the dark energy from the holographic connection to the small l CMB suppression, an opposite result is derived, i.e. it implies the best fit result is $c = 2.1$ [16]. We see explicitly that these results are very incompatible. In order to demonstrate the tremendous difference between these cases in the time evolution of the universe, we perform a statefinder diagnostic to these cases.

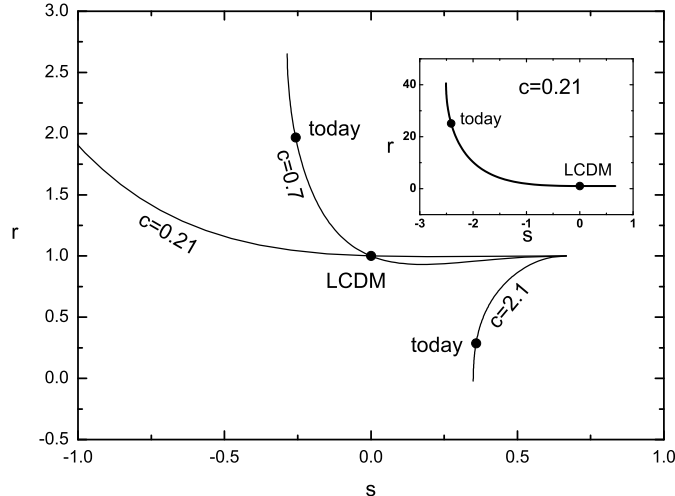


FIG. 3. The statefinder diagrams $r(s)$ for holographic dark energy model in the cases of $c = 0.21, 0.7$ and 2.1 , respectively. The inset shows the complete curve for the case $c = 0.21$. The coordinates of today are $(-2.41, 25.13)$, $(-0.26, 1.97)$ and $(0.36, 0.29)$, corresponding to the cases $c = 0.21, 0.7$ and 2.1 , respectively.

We plot in Fig.3 the statefinder diagrams $r(s)$ for the holographic dark energy model in three cases of which the parameter c is taken to be $0.21, 0.7$ and 2.1 , respectively. This figure strikingly demonstrates that the evolution trajectories of these cases in the $s - r$ plane are tremendously different. We see that the evolutionary trends of cases $c < 1$ and $c > 1$ are upward and downward, respectively. In particular, we notice that for the $c = 0.21$ case, r can arrive at a very large value, about 40, as shown in the inset in Fig.3. For the situations of $c < 1$, the trajectories pass through the LCDM fixed point; while for the $c > 1$ cases, the tracks never reach the LCDM fixed point. The coordinates of today's statefinders are $(-2.41, 25.13)$, $(-0.26, 1.97)$ and $(0.36, 0.29)$, corresponding to the cases $c = 0.21, 0.7$ and 2.1 , respectively. From this figure it can be seen that the model universes at today corresponding to $c = 0.21$ and $c = 0.7$ have evolved through the LCDM fixed point. It is clear that the present values of the statefinders, r and s , can be used to distinguish the holographic dark energy models with different values of c . Obviously, the distances between these cases can also be easily measured. It is remarkable that, from the statefinder viewpoint, the parameter c plays an important role in this model, and it determines the evolution behavior as well as the ultimate fate of the model universe. We hope that the future high precision experiments (e.g. SNAP) may provide sufficiently large amount of precise data to be capable of determining the value of c .

In summary, we study in this paper the holographic dark energy model from the statefinder viewpoint. We plot the evolutionary trajectories of this model in the statefinder parameter-planes. The statefinder diagrams characterize the properties of the holographic dark energy and show the discrimination between this model and other dark energy models.

The statefinder diagnostic can also be performed to the holographic dark energy model in cases of different c , in this paper we chose three fit results as example, which indicates that the value of c determines the evolution behavior and the fate of the universe. We hope that the future large amount of data on high- z Type Ia supernovae may be capable of determining the statefinder parameters and consequently shed light on the nature of dark energy.

ACKNOWLEDGMENTS

This work was supported in part by the Natural Science Foundation of China (Grant No. 10375072).

REFERENCES

- [1] A. G. Riess *et al.*, *Astron. J.* **116** (1998) 1009 [astro-ph/9805201](#); S. Perlmutter *et al.*, *Astrophys. J.* **517** (1999) 565 [astro-ph/9812133](#).
- [2] C. L. Bennett *et al.*, *Astrophys. J. Suppl.* **148** (2003) 1 [astro-ph/0302207](#); D. N. Spergel *et al.*, *Astrophys. J. Suppl.* **148** (2003) 175 [astro-ph/0302209](#); H. V. Peiris *et al.*, *Astrophys. J. Suppl.* **148** (2003) 213 [astro-ph/0302225](#).
- [3] S. Weinberg, *Rev. Mod. Phys.* **61** (1989) 1; S. M. Carroll, *Living Rev. Rel.* **4** (2001) 1 [astro-ph/0004075](#); P. J. E. Peebles and B. Ratra, *Rev. Mod. Phys.* **75** (2003) 559 [astro-ph/0207347](#); T. Padmanabhan, *Phys. Rept.* **380** (2003) 235 [hep-th/0212290](#).
- [4] C. Wetterich, *Nucl. Phys. B* **302** (1988) 668; P. J. E. Peebles and B. Ratra, *Astrophys. J.* **325** (1988) L17; B. Ratra and P. J. E. Peebles, *Phys. Rev. D* **37** (1988) 3406; J. A. Frieman, C. T. Hill, A. Stebbins and I. Waga, *Phys. Rev. Lett.* **75** (1995) 2077 [astro-ph/9505060](#); M. S. Turner and M. White, *Phys. Rev. D* **56** (1997) 4439 [astro-ph/9701138](#); R. R. Caldwell, R. Dave and P. J. Steinhardt, *Phys. Rev. Lett.* **80** (1998) 1582 [astro-ph/9708069](#); A. R. Liddle and R. J. Scherrer, *Phys. Rev. D* **59** (1999) 023509 [astro-ph/9809272](#); I. Zlatev, L. Wang and P. J. Steinhardt, *Phys. Rev. Lett.* **82** (1999) 896 [astro-ph/9807002](#); P. J. Steinhardt, L. Wang and I. Zlatev, *Phys. Rev. D* **59** (1999) 123504 [astro-ph/9812313](#); D. F. Torres, *Phys. Rev. D* **66** (2002) 043522 [astro-ph/0204504](#).
- [5] J. D. Bekenstein, *Phys. Rev. D* **7** (1973) 2333; J. D. Bekenstein, *Phys. Rev. D* **9** (1974) 3292; J. D. Bekenstein, *Phys. Rev. D* **23** (1981) 287; J. D. Bekenstein, *Phys. Rev. D* **49** (1994) 1912; S. W. Hawking, *Commun. Math. Phys.* **43** (1975) 199; S. W. Hawking, *Phys. Rev. D* **13** (1976) 191.
- [6] A. G. Cohen, D. B. Kaplan and A. E. Nelson, *Phys. Rev. Lett.* **82** (1999) 4971 [hep-th/9803132](#).
- [7] G. 't Hooft, [gr-qc/9310026](#); L. Susskind, *J. Math. Phys.* **36** (1994) 6377 [hep-th/9409089](#).
- [8] S. D. H. Hsu, *Phys. Lett. B* **594** (2004) 13 [hep-th/0403052](#).
- [9] M. Li, *Phys. Lett. B* **603** (2004) 1 [hep-th/0403127](#).
- [10] K. Ke and M. Li, *Phys. Lett. B* **606** (2005) 173 [hep-th/0407056](#); S. Hsu and A. Zee, [hep-th/0406142](#); Y. Gong, *Phys. Rev. D* **70** (2004) 064029 [hep-th/0404030](#); Y. S. Myung, *Phys. Lett. B* **610** (2005) 18; Y. S. Myung, [hep-th/0501023](#); H. Kim, H. W. Lee and Y. S. Myung, [hep-th/0501118](#); Y. S. Myung, [hep-th/0502128](#).
- [11] Q. G. Huang and M. Li, *JCAP* **0408** (2004) 013 [astro-ph/0404229](#); Q. G. Huang and M. Li, *JCAP* **0503** (2005) 001 [hep-th/0410095](#).
- [12] Q. G. Huang and Y. Gong, *JCAP* **0408** (2004) 006 [astro-ph/0403590](#).

- [13] Y. Gong, B. Wang and Y. Z. Zhang, [hep-th/0412218](#).
- [14] H. C. Kao, W. L. Lee and F. L. Lin, [astro-ph/0501487](#).
- [15] K. Enqvist and M. S. Sloth, *Phys. Rev. Lett.* **93** (2004) 221302 [hep-th/0406019](#). K. Enqvist, S. Hannestad and M. S. Sloth, *JCAP* **0502** (2005) 004 [astro-ph/0409275](#).
- [16] J. Shen, B. Wang, E. Abdalla and R. K. Su, [hep-th/0412227](#).
- [17] E. Elizalde, S. Nojiri, S. D. Odintsov and P. Wang, [hep-th/0502082](#).
- [18] V. Sahni, T. D. Saini, A. A. Starobinsky and U. Alam, *JETP Lett.* **77** (2003) 201 [astro-ph/0201498](#).
- [19] U. Alam, V. Sahni, T. D. Saini and A. A. Starobinsky, *Mon. Not. Roy. ast. Soc.* **344** (2003) 1057 [astro-ph/0303009](#).
- [20] V. Gorini, A. Kamenshchik and U. Moschella, *Phys. Rev. D* **67** (2003) 063509 [astro-ph/0209395](#).
- [21] W. Zimdahl and D. Pavon, *Gen. Rel. Grav.* **36** (2004) 1483 [gr-qc/0311067](#).
- [22] X. Zhang, *Phys. Lett. B* **611** (2005) 1 [astro-ph/0503075](#).
- [23] B. Feng, X. Wang and X. Zhang, *Phys. Lett. B* **607** (2005) 35 [astro-ph/0404224](#).
- [24] *e.g.* S. Nesseris and L. Perivolaropoulos, *Phys. Rev. D* **70** (2004) 043531 [astro-ph/0401556](#); R. A. Daly and S. G. Djorgovski, *Astrophys. J.* **612** (2004) 652 [astro-ph/0403664](#); U. Alam, V. Sahni, and A. A. Starobinsky, *JCAP* 0406 (2004) 008 [astro-ph/0403687](#); D. Huterer and A. Cooray, *Phys. Rev. D* **71** (2005) 023506 [astro-ph/0404062](#); S. W. Allen, R. W. Schmidt, H. Ebeling, A. C. Fabian, and L. van Speybroeck, *Mon. Not. Roy. Astron. Soc.* **353** (2004) 457 [astro-ph/0405340](#); T. R. Choudhury and T. Padmanabhan, *Astron. Astrophys.* **429** (2005) 807 [astro-ph/0311622](#); H. K. Jassal, J. S. Bagla and T. Padmanabhan, *Mon. Not. Roy. Astron. Soc. Lett.* **356** (2005) L11 [astro-ph/0404378](#); S. Hannestad and E. Mortsell, *JCAP* **0409** (2004) 001 [astro-ph/0407259](#); P. S. Corasaniti, M. Kunz, D. Parkinson, E. J. Copeland and B. A. Bassett, *Phys. Rev. D* **70** (2004) 083006 [astro-ph/0406608](#); D. A. Dicus and W. W. Repko, *Phys. Rev. D* **70** (2004) 083527 [astro-ph/0407094](#); B. A. Bassett, P. S. Corasaniti, and M. Kunz, *Astrophys. J.* **617** (2004) L1 [astro-ph/0407364](#).
- [25] For relevant studies see *e.g.* S. Nojiri and S. D. Odintsov, *Phys. Lett. B* **562** (2003) 147 [hep-th/0303117](#); S. Nojiri and S. D. Odintsov, *Phys. Lett. B* **599** (2004) 137 [astro-ph/0403622](#); E. Elizalde, S. Nojiri and S. D. Odintsov, *Phys. Rev. D* **70** (2004) 043539 [hep-th/0405034](#); Y. H. Wei and Y. Tian, *Class. Quant. Grav.* **21** (2004) 5347 [gr-qc/0405038](#); C. Csaki and N. Kaloper, [astro-ph/0409596](#); Y. Wang, J. M. Kratochvil, A. Linde, M. Shmakova, *JCAP* **0412** (2004) 006 [astro-ph/0409264](#); V. K. Onemli and R. P. Woodard, *Class. Quant. Grav.* **19** (2002) 4607 [gr-qc/0204065](#);

T. Brunier, V. K. Onemli, R. P. Woodard, *Class. Quant. Grav.* **22** (2005) 59-84 [gr-qc/0408080](#); B. McInnes, *JHEP* **0410** (2004) 018 [hep-th/0407189](#); G. Allemandi, A. Borowiec and M. Francaviglia, *Phys. Rev. D* **70** (2004) 103503 [hep-th/0407090](#); E. Babichev, V. Dokuchaev and Y Eroshenko, *Class. Quant. Grav.* **22** (2005) 143 [astro-ph/0407190](#); A. Vikman, *Phys. Rev. D* **71** (2005) 023515 [astro-ph/0407107](#); Z. H. Zhu and J. S. Alcaniz *Astrophys. J.* **620** (2005) 7 [astro-ph/0404201](#); V. K. Onemli and R. P. Woodard, [gr-qc/0406098](#); S. D. H. Hsu, A. Jenkins and M. B. Wise, *Phys. Lett. B* **597** (2004) 270 [astro-ph/0406043](#); G. Chen and B. Ratra, *Astrophys. J.* **612** (2004) L1 [astro-ph/0405636](#); T. Padmanabhan, [astro-ph/0411044](#); B. Feng, M. Li, Y. Piao and X. Zhang, [astro-ph/0407432](#); J. Xia, B. Feng and X. Zhang, [astro-ph/0411501](#); S. Nojiri, S. D. Odintsov and S. Tsujikawa, [hep-th/0501025](#).

[26] Z. Guo, Y. Piao, X. Zhang and Y. Zhang, *Phys. Lett. B* **608** (2005) 177 [astro-ph/0410654](#); X. Zhang, H. Li, Y. Piao and X. Zhang, [astro-ph/0501652](#).